

See discussions, stats, and author profiles for this publication at: <https://www.researchgate.net/publication/230717943>

# Carbon-Doped TiO<sub>2</sub> and Carbon, Tungsten-Codoped TiO<sub>2</sub> Through Sol-Gel Processes in the Presence of Melamine Borate: Reflections Through Photocatalysis

ARTICLE in THE JOURNAL OF PHYSICAL CHEMISTRY C · JULY 2012

Impact Factor: 4.77 · DOI: 10.1021/jp303645p

CITATIONS

33

READS

76

8 AUTHORS, INCLUDING:



Michael Jon Mattle

École Polytechnique Fédérale de Lausanne

8 PUBLICATIONS 82 CITATIONS

SEE PROFILE



Mahfujur Rahman

University College Dublin

42 PUBLICATIONS 473 CITATIONS

SEE PROFILE



James M D Macelroy

University College Dublin

116 PUBLICATIONS 1,680 CITATIONS

SEE PROFILE



K. Ravindranathan Thampi

École Polytechnique Fédérale de Lausanne

133 PUBLICATIONS 2,583 CITATIONS

SEE PROFILE

# Carbon-Doped TiO<sub>2</sub> and Carbon, Tungsten-Codoped TiO<sub>2</sub> through Sol–Gel Processes in the Presence of Melamine Borate: Reflections through Photocatalysis

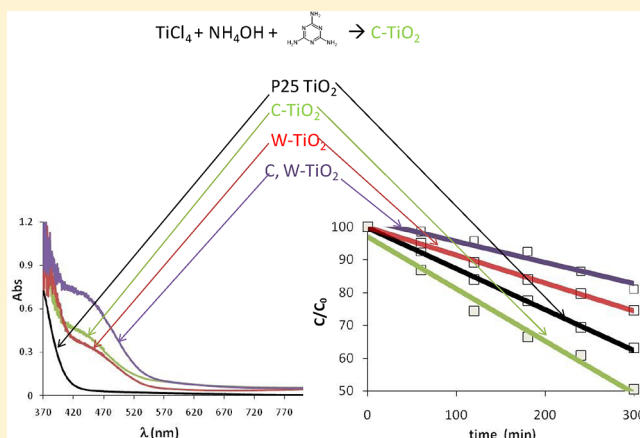
Elaine M. Neville,<sup>†</sup> Michael J. Mattle,<sup>§</sup> David Loughrey,<sup>‡</sup> Bashyam Rajesh,<sup>§</sup> Mahfujur Rahman,<sup>‡</sup> J.M. Don MacElroy,<sup>‡</sup> James A. Sullivan,<sup>\*,†</sup> and K. Ravindranathan Thampi<sup>\*,§,‡,||</sup>

<sup>†</sup>UCD School of Chemistry and Chemical Biology and <sup>‡</sup>UCD School of Chemical and Bioprocess Engineering, SFI Strategic Research Cluster in Solar Energy Conversion, Belfield, Dublin 4, Ireland.

<sup>§</sup>Laboratory of Photonics and Interfaces, ISIC, École Polytechnique Fédérale de Lausanne, CH-1015, Lausanne, Switzerland.

## Supporting Information

**ABSTRACT:** A series of C-doped, W-doped, and C,W-codoped TiO<sub>2</sub> samples have been prepared using modified sol–gel techniques. Reproducible inexpensive C-doping arises from the presence of melamine borate in a sol–gel mixture, whereas W-doping is from the addition of tungstic acid to the sol. The materials have been characterized using elemental analysis, N<sub>2</sub> physisorption (BET), thermogravimetric analysis, X-ray diffraction, Raman, X-ray photoelectron, UV–vis spectroscopies, and photocatalytic activity measurements. Doping C and W independently results in an increased absorbance in the visible region of the spectrum with a synergistic effect in increased absorbance when both elements are codoped. The increased visible-light absorbance of the W-doped or codoped materials is not reflected in photocatalytic activity. Visible-light-induced photocatalytic activity of C-doped material was superior to that of an undoped catalyst, paving the way for its application under only visible-light irradiation conditions. A significant fraction of the spectral red shift commonly observed with doped catalysts might be due to the formation of color centers as a result of defects associated with oxygen vacancies, and bandgap-related narrowing or intragap localization of dopant levels are not the only factors responsible for enhanced visible-light absorption in doped photocatalysts. Furthermore, bandgap narrowing through increases in the energy of the valence band may actually decrease photo-oxidation activity through a curtailment of one route of oxidation.



## 1. INTRODUCTION

The initial step of all photocatalytic processes promoted by semiconductor materials involves the absorption of a photon of energy  $\geq E_g$  (bandgap), which promotes an electron from its valence band (VB) to the conduction band (CB). This generates an electron ( $e^-$ ) in the CB and leaves behind a hole ( $h^+$ ) in the VB.<sup>1,2</sup> The former can act as a reductant, and the latter can act as an oxidant in the different photocatalytic and photo-synthetic processes being considered, for example, water splitting to hydrogen and oxygen,<sup>3,4</sup> pollutant oxidation,<sup>5,6</sup> or aqueous phase reforming of organic compounds.<sup>7,8</sup> TiO<sub>2</sub> is the ubiquitous photocatalyst due to its low cost, biocompatibility, its chemical and biochemical stability, and its interesting photocatalytic activity.<sup>9,10</sup>

One of the major limitations associated with the use of TiO<sub>2</sub> for solar driven photocatalysis is that the  $E_g$  of pure anatase TiO<sub>2</sub> (3.2 eV) is too large for visible light to promote an electron from the VB to the CB.<sup>4</sup> In effect, this limits the use of TiO<sub>2</sub> as a photocatalyst to only harvesting the UV component

of the terrestrially available sunlight. Because the majority of solar radiation incident on the surface of the planet has insufficient energy to initiate TiO<sub>2</sub> photocatalysis, the efficiency of such solar-driven processes is significantly compromised.

One way to counter this limitation and shift absorbance into the visible region of the solar spectrum is to alter the bandgap of TiO<sub>2</sub> through selective doping. A wide variety of dopants have been studied including both metallic and nonmetallic elements.<sup>11–24</sup> Doping of TiO<sub>2</sub> with nonmetals (specifically C and N) has attracted significant attention.<sup>11,12,14,15,17–19,21,23–25</sup> Co-doping of C and N has also been investigated.<sup>12</sup> There are several reports that combine the two approaches, that is, metal and nonmetal ions-codoped TiO<sub>2</sub> photocatalysts; for example, codoping with nitrogen and various metal ions, has been studied<sup>26,27</sup> and to a lesser extent carbon and tungsten codoping.<sup>28</sup>

Received: April 16, 2012

Revised: July 10, 2012

Published: July 13, 2012

In this work, we have prepared and characterized a series of carbon-doped, tungsten-doped, and carbon–tungsten codoped  $\text{TiO}_2$  catalysts. The preparations have involved sol–gel procedures using  $\text{TiCl}_4$  and tungstic acid precursors in which the carbon source has been a melamine borate salt added to the preparation mixture. Melamine salts have been chosen as the source of the carbon dopant due to the fact that their deep oxidation requires relatively high temperatures. Therefore, following the formation of  $\text{TiO}_2$  from calcination of the sol–gel derived precursor, dopant amounts of carbon can remain within the lattice. The formation of the materials during calcination has been studied using TGA with residual gas analysis, whereas the textural properties of the final powders have been characterized using  $\text{N}_2$  physisorption. Their morphologies have been confirmed using XRD and Raman spectroscopy. The carbon levels within the samples have been analyzed using elemental analysis while the nature of the carbon doping (near the surfaces of the  $\text{TiO}_2$  particles) has been evaluated using XPS. The electronic properties of the materials have been monitored using diffuse reflectance UV–visible spectroscopy and their activities have been probed using a model photocatalytic reaction and the results interpreted based on different reactions involving the photogenerated electrons and holes.

## 2. EXPERIMENTAL SECTION

**Preparation of  $\text{TiO}_2$ , C-Doped  $\text{TiO}_2$ , and W,C-Codoped  $\text{TiO}_2$ .**  $\text{TiO}_2$  and doped  $\text{TiO}_2$  materials were formed using hydrolysis of  $\text{TiCl}_4$  (followed by condensation) to form the  $\text{X}_3\text{Ti}-\text{O}-\text{TiX}_3$  lattices (where X represents OH or  $-\text{O}-\text{TiX}_3$  groups). In the case of C-doped catalysts the carbon was derived from melamine borate, which was added to the mixture prior to hydrolysis. Tungsten doping was introduced through the addition of tungstic acid to the mixture.

In a typical synthesis of C-doped  $\text{TiO}_2$ , 3.4 g of melamine borate (Budenheim, Germany) was dissolved in 0.5 L of deionized water under constant stirring at room temperature. After 24 h, the solution was filtered through Whatman grade 1 filter paper. Eleven mL of  $\text{TiCl}_4$  ( $\geq 99.0\%$  (AT), Fluka) was slowly dissolved in 1.5 L of deionized water at 2–4 °C. To this solution, various aliquots (3.5, 7, and 14 mL) of melamine borate solution were added and stirred for 30 min. Nominally (assuming all carbon added remained in the final prepared material), this represents C doping at levels of 1, 2, and 4%, respectively (see below). A 2.5 M solution of ammonium hydroxide (made through dilution of a 26% solution, Riedel-de Haen, Germany) was added dropwise until pH 5 was reached. This resulted in precipitation of the  $\text{TiO}_2$  precursor from the solution. The precipitate obtained was allowed to settle overnight before being filtered through Whatman grade 1 filter paper and washed repeatedly with warm deionized water (to eliminate  $\text{Cl}^-$  from the solid). The removal of  $\text{Cl}^-$  was confirmed using a standard  $\text{AgNO}_3$  precipitation test. The solid was then dried at 80 °C overnight. The resultant material was ground into fine powder and calcined at 400 °C for various lengths of time (1, 3, 15 h, etc.).

The nominal levels of doped C mentioned above assume that all of the carbon in the melamine borate remains in the material following calcination. Obviously this is not the case as significant portions are removed during the calcination step or remain in the supernatant fluid as the precatalyst material crystallizes from solution. The actual levels of C remaining within or upon the materials were determined using microanalysis. The final products were yellow powders.

Similarly, a series of W-doped catalysts was prepared using different concentrations of tungstic acid (99%, Aldrich) within the precipitating mixture.<sup>16</sup> The codoped  $\text{TiO}_2$  materials were synthesized following the addition of both tungstic acid and melamine borate to the mixture. We produced 1, 5, and 10% W- $\text{TiO}_2$  (mass %). The W-containing material was dried at 80 °C overnight and then ground to a fine powder before being calcined for 15 h at 400 °C. The materials produced were again yellow in color.

**Analysis of the Calcination Process.** A Hiden analytical HPR20-QIC atmospheric gas analysis system coupled to a thermogravimetric analyzer (TA Instruments, TGA 500) was used in the analysis of the material calcination steps. The dried precatalysts were held in a flow of air ( $100 \text{ mL min}^{-1}$ ), and while the temperature was raised using a linear rate of increase ( $20 \text{ }^\circ\text{C min}^{-1}$ ) the exit gas was continuously analyzed by mass spectrometry. Profiles of the evolved  $\text{CO}_2$ , NO, and  $\text{H}_2\text{O}$  were recorded as a function of temperature. Typically, an aliquot of 50 mg of the dried precursor was loaded onto a balance within the TGA. The sample was held in a flow of air at room temperature for 1 h. The temperature was then ramped at a rate of  $20 \text{ }^\circ\text{C min}^{-1}$  to 400 °C and held at this temperature for 1 h (to mimic the calcination process) or ramped  $20 \text{ }^\circ\text{C min}^{-1}$  up to 1000 °C (to analyze the material following calcination). The temperature of removal and the extent of removal (through combustion) of the various carbon-containing species present in the materials both during and following calcination were monitored in this way.

**Catalyst Characterizations.** Diffuse Reflectance UV–vis spectroscopy (DRS) was carried out using an Analytik Jena Specord 210 spectrometer equipped with an integrating sphere attachment for measurement of spectra from powder samples. Band gaps were estimated by drawing a tangent to the high-energy feature and approximating a bandgap energy from the wavelength at which the tangent intercepts a line with an absorbance value of zero. Raman spectra were obtained using a SENTERRA dispersive Raman microscope (Bruker Optics) with a 785 nm laser. Powder XRD patterns were collected using a Siemens D500 Kristalloflex using  $\text{Cu K}\alpha$  radiation.  $\text{N}_2$  physisorption isotherms were collected on a Quantachrome Nova 2000e. X-ray photoelectron spectroscopy (XPS) was carried out with a Kratos AXIS 165 spectrometer using a monochromatic X-ray source (Al  $\text{K}\alpha$  1486.58 eV). Elemental analysis was performed using various techniques: C, H, N analysis was carried out with a CE-440 elemental analyzer (Exeter Analytical) using thermal conductivity detection for measurement following combustion and reduction.  $\text{Cl}^-$  analysis was performed using oxygen flask combustion, followed by filtration. W analysis and further  $\text{Cl}^-$  analysis was carried out using EDX with a FEI Quanta 3D FEG DualBeam (FEI, Hillsboro, OR) SEM coupled to an EDAX EDX APOLLO XV silicon drift detector.

**Photocatalytic Activity Measurements.** Photocatalytic activity of the materials was tested by investigating the initial photocatalytic degradation of 4-chlorophenol solutions. We dispersed 80 mg of photocatalyst powder in 40 mL of a 0.5 mM solution of 4-chlorophenol. The mixture was sonicated for 15 min before being purged with air for 5 min. Samples were stirred in the dark for 30 min to reach an adsorption–desorption equilibrium. Irradiation was carried out in an Atlas Suntest CPS (AM1.5 G) solar simulator unit with (when required) a UV filter film ( $\lambda > 410 \text{ nm}$ ). Samples were extracted hourly for 5 h, and the degradation (complete mineralization) of 4-chlorophenol

was monitored using total organic carbon (TOC) analysis (Shimadzu TOC V-CPH).

### 3. RESULTS AND DISCUSSION

In most doped photocatalyst studies, there is an uncertainty as to whether the dopant is truly in a doped state and, when truly doped, whether it resides preferentially in the  $\text{TiO}_2$  bulk or on the surface. Depending on these variations, the photocatalytic reaction mechanisms would show changes. Therefore, the levels of dopants were analyzed by both elemental analysis and XPS in attempts to differentiate whether all carbon found in the sample is of a doped nature and whether they are selectively enriched on the surface with respect to the bulk. The XPS measurements (see later), besides providing solely the surface concentration, is also able to give an insight into the nature of the carbon species located on the surface.

In all cases (for doped and undoped samples), elemental analysis shows that the total level of carbon in the samples is between 0.01 and 0.03%. There is no relationship between the amount of melamine salt used in the preparation and the eventual measured concentration of C in the material; that is, C- $\text{TiO}_2$  materials showed similar levels of carbon content irrespective of the levels of melamine borate added initially to the preparation mixture, and similar levels of carbon were noted on samples that nominally were undoped. This suggests that the concentrations of surface carbon, including carbonate on the materials, for example, arising from adsorption of  $\text{CO}_2$ , are significantly higher than the levels of carbon dopants incorporated in the bulk. However, as noted by XPS (see later), the nature and dispersion of carbon on the doped samples differs from that in the undoped samples. Table 1 shows the measured levels of W in the

**Table 1. Measured [C] and [W], Absorption Onsets, and Bandgap Estimates for the Doped  $\text{TiO}_2$  Materials<sup>a</sup>**

theoretical % doping	% C (elemental analysis)	% W (EDX)	absorption onset (nm)	bandgap (eV)
P25 $\text{TiO}_2$	0.03		410	3.02
1% C- $\text{TiO}_2$ , 1 h	0.03		425	2.92
2% C- $\text{TiO}_2$ , 1 h	0.02		425	2.92
4% C- $\text{TiO}_2$ , 1 h	0.03		430	2.88
1% C- $\text{TiO}_2$ , 3 h	0.02		430	2.88
2% C- $\text{TiO}_2$ , 3 h	0.02		430	2.88
4% C- $\text{TiO}_2$ , 3 h	0.03		430	2.88
1% W- $\text{TiO}_2$	0.01	1.40	433	2.86
5% W- $\text{TiO}_2$	0.02	5.79	438	2.83
10% W- $\text{TiO}_2$	0.01	9.80	442	2.80
1% C, 1% W- $\text{TiO}_2$	0.02	1.21	438	2.83
1% C, 5% W- $\text{TiO}_2$	0.01	5.15	450	2.76
1% C, 10% W- $\text{TiO}_2$	0.02	7.11	465	2.67
2% C, 1% W- $\text{TiO}_2$	0.01	1.27	442	2.81
2% C, 5% W- $\text{TiO}_2$	0.01	4.19	460	2.70
2% C, 10% W- $\text{TiO}_2$	0.01	10.24	470	2.64
4% C, 1% W- $\text{TiO}_2$	0.01	1.23	435	2.85
4% C, 5% W- $\text{TiO}_2$	0.02	3.83	465	2.67
4% C, 10% W- $\text{TiO}_2$	0.02	7.10	480	2.58

<sup>a</sup>Indicated times refer to the length of the calcination step for the relevant materials.

W-doped samples as well as the absorption onsets and calculated bandgaps of the materials. The tungsten and codoped samples showed a trend for slightly reduced levels of carbon (0.01 to 0.02 mass %). This may partially be due to the

incorporation of the heavier  $\text{W}^{6+}$  ion influencing the relative mass % values.

Thermogravimetric-mass spectrometry (TGA-MS) analysis was carried out on the catalyst precursor to mimic the calcination of the material. The precipitate from a C- $\text{TiO}_2$  preparation (with a nominal 4% C-doping) was heated to 400 °C in air. These TGA and evolved gas profiles (Figure 1a,b) show a range

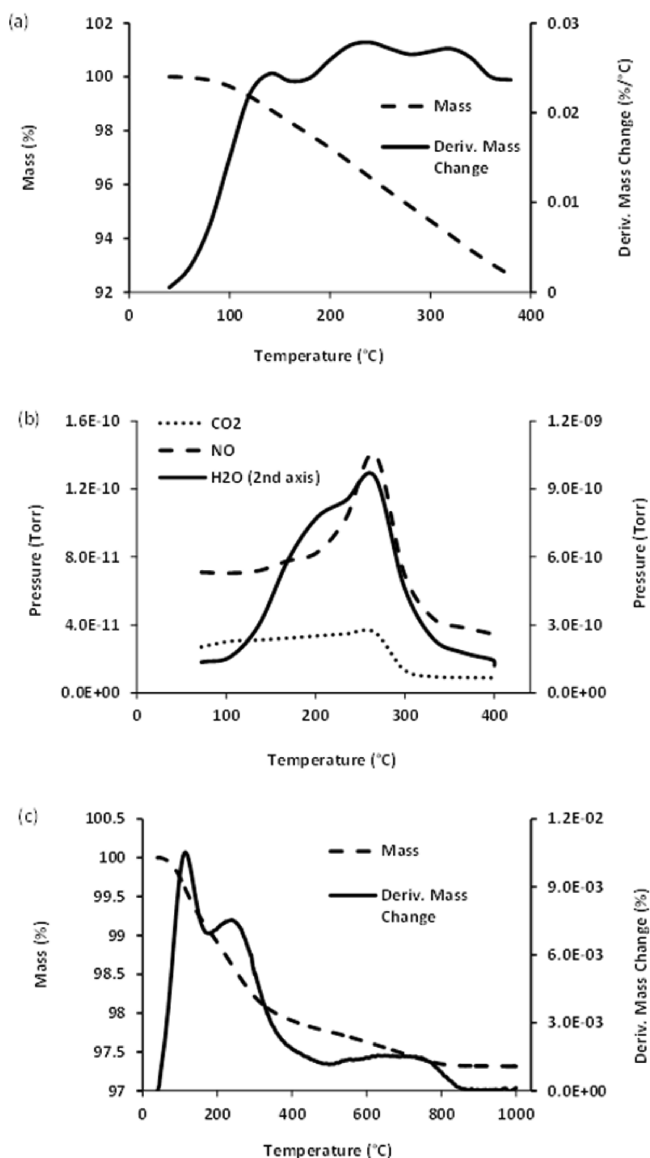


**Figure 1.** (a) TGA and DTGA profiles measured during the calcination of the pre-catalyst to 400 °C, (b) evolved gas analysis from the same experiment, and (c) TGA and DTGA profiles of an already calcined sample of C- $\text{TiO}_2$ . All catalysts are with a nominal loading of 4% C based on the amount of melamine borate added initially.

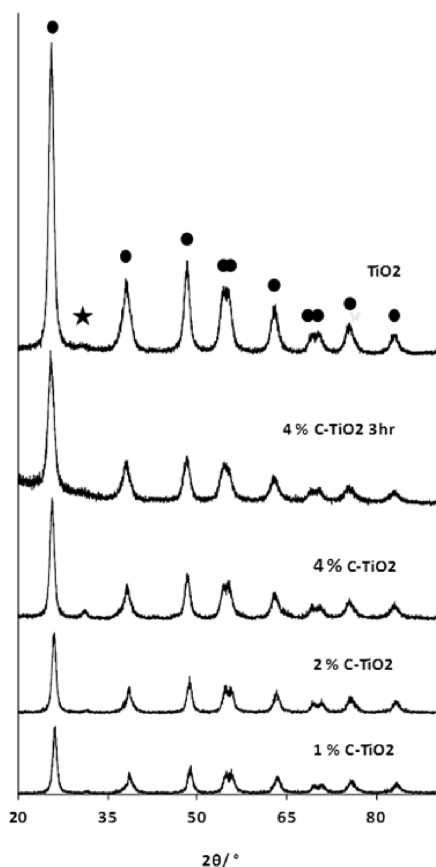
of oxidation events with the release of  $\text{CO}_2$ ,  $\text{H}_2\text{O}$ , and NO (from the combustion of melamine in the pre-catalyst) peaking at a temperature of ~260 °C. This confirms that significant amounts of melamine are still present in the precipitated material and large amounts of these are removed from the catalyst during calcination.

Figure 1c shows the results of a TGA carried out on a catalyst that had previously been calcined at 400 °C for 1 h. An approximate 2% weight change is observed at temperatures lower than



400 °C. This presumably is due to the removal of adsorbed or condensed species on the surface. A further weight change is observed at higher temperature (600–800 °C) that may be attributable to removal of the carbon dopant or oxygen loss resulting in the formation of Magnéli phase  $\text{TiO}_{2-x}$  suboxides.<sup>29</sup> No  $\text{CO}_2$  was observed in the exit gas concurrent with this peak (although any  $\text{CO}_2$  formed from the combustion of the small amounts of dopants would be difficult to detect under these conditions). Following the thermal treatment, the catalyst acquired a light-gray color.

XRD patterns were obtained to determine the crystal phase of the photocatalysts. Figure 2 shows the XRD patterns of the



**Figure 2.** XRD patterns of C-doped  $\text{TiO}_2$ . Samples with nominal dopant levels of 1, 2, and 4% calcined at 400 °C for 1 h and a sample with a nominal dopant level of 4% calcined at 400 °C for 3 h (upper profile): ● indicates anatase and \* indicates brookite phases.

C-doped  $\text{TiO}_2$  materials series calcined at 400 °C for 1 h. The powder shows anatase phase peaks (JCPDS: No 21-1272). The nominally 4% carbon  $\text{TiO}_2$  also displays an additional peak at  $\sim 30^\circ$  confirming trace levels of brookite formation (JCPDS: No 29-1360).<sup>30</sup> After a 3 h calcination step, this peak disappears (see Figure 2).

XRD patterns of W-doped  $\text{TiO}_2$  materials (with different levels of W incorporated) and the profiles collected from C,W-codoped materials are shown in Figure 3. In the case of the solely W-doped samples, some rutile peaks are also evident (■) where solid square refers to the rutile peaks in Figure 3. However, tungsten incorporation has been reported to retard the transition from anatase to rutile,<sup>31,32</sup> and our result seems to contradict this observation. Peaks relating to the rutile phase are, however, absent in the codoped materials.

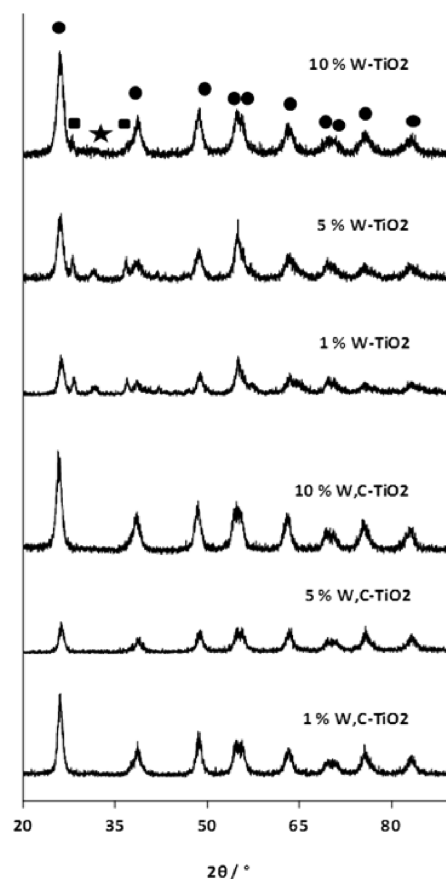


**Figure 3.** XRD profiles of W-doped  $\text{TiO}_2$  samples with nominal loadings of 1, 5, and 10% W- and C,W-codoped samples containing nominally 4% C and 1, 5, and 10% W. ● indicates anatase, whereas ■ indicates rutile and \* indicates brookite phases.

Raman spectra (not shown) also confirm the presence of the anatase phase in all of the samples, that is, six Raman active modes were noted ( $A_{1g}$  (519  $\text{cm}^{-1}$ ),  $B_{1g}$  (399 and 519  $\text{cm}^{-1}$ ), and  $E_g$  (144, 197, and 639  $\text{cm}^{-1}$ )), all consistent with the presence of the anatase phase. The W- $\text{TiO}_2$  materials also showed additional smaller Raman active modes at 232, 446, and 609  $\text{cm}^{-1}$ , confirming the presence of the rutile phase.

The crystallite particle size, as calculated using the Scherrer equation<sup>33</sup> applied to the XRD peak (101) at  $2\theta = \sim 25^\circ$  (with shape factor  $K = 0.94$ ), and surface area of the various photocatalysts, as determined using BET, are summarized in Table 2. As expected, an increase in calcination time of the C- $\text{TiO}_2$  materials from 1 to 3 h resulted in an increase in crystalline particle size from approximately 6 to 10 nm due to greater sintering of the material.

Increasing the concentration of melamine used during preparation also slightly affected the crystalline particle size of the C- $\text{TiO}_2$  materials. Materials with nominally 4% C that had been calcined for 3 h had particle sizes of  $\sim 9$  nm, whereas those with lower nominal [C] were slightly larger, with particle sizes of  $\sim 10$  nm. This may be due to dissimilar boundaries created by carbon doping,<sup>34</sup> resulting in slower rates of crystal growth and hence smaller crystallite size when the heating is prolonged for a longer time.

The W-containing materials, despite having an increased calcination time of 15 h, did not show any further increase in crystallite size compared with C-doped materials. This may be due to W incorporation slowing crystal growth rates,<sup>16,31,32</sup>

**Table 2. Crystalline Particle Size (Estimated Using the Scherrer Equation), BET Surface Areas and Pore Volumes of Representative Samples of C-Doped, W-Doped and C,W-Codoped TiO<sub>2</sub> Materials**

theoretical % doping	particle size (nm)	surface area (m <sup>2</sup> g <sup>-1</sup> )	pore volume (cc/g)
P25 TiO <sub>2</sub>	13.8 (anatase)	58.0	0.09
1% C-TiO <sub>2</sub> , 1 h	6.3	141.1	1.40
2% C-TiO <sub>2</sub> , 1 h	6.5	149.2	1.60
4% C-TiO <sub>2</sub> , 1 h	6.4	148.2	1.80
1% C-TiO <sub>2</sub> , 3 h	10.3	105.0	0.33
2% C-TiO <sub>2</sub> , 3 h	10.1	127.0	0.38
4% C-TiO <sub>2</sub> , 3 h	9.4	123.1	0.37
1% W-TiO <sub>2</sub>	7.8	89.8	0.20
5% W-TiO <sub>2</sub>	6.7	99.2	0.17
10% W-TiO <sub>2</sub>	5.9	123.1	0.20
1% C, 1% W-TiO <sub>2</sub>	8.2	104.9	0.29
1% C, 5% W-TiO <sub>2</sub>	7.8	109.8	0.26
1% C, 10% W-TiO <sub>2</sub>	8.3	141.0	0.37
2% C, 1% W-TiO <sub>2</sub>	9.5	106.5	0.34
2% C, 5% W-TiO <sub>2</sub>	9.5	136.8	0.33
2% C, 10% W-TiO <sub>2</sub>	7.7	137.1	0.30
4% C, 1% W-TiO <sub>2</sub>	9.3	104.5	0.30
4% C, 5% W-TiO <sub>2</sub>	8.0	125.5	0.29
4% C, 10% W-TiO <sub>2</sub>	7.4	152.1	0.32

which could be attributed to increased formation energies as evidenced by higher Madelung constants. Furthermore, an increase in nominal levels of W dopant from 1 to 10% also resulted in a decrease in particle size from approximately 8 to 6 nm and an increase in surface area.

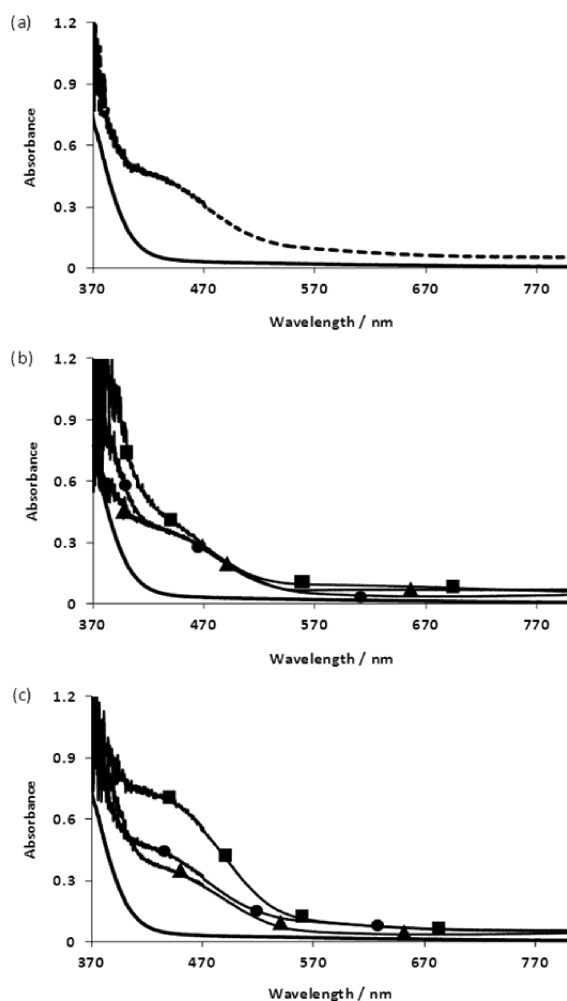
Particle size and surface area measurements of the codoped materials, in general, showed little change with increased levels of melamine borate used in the preparation mixture but did display a slight decrease in crystallite size upon increased incorporation of W dopant. Again, surface areas increased with decreased particle size.

Figure 4 shows the UV–vis diffuse reflectance spectra (DRS) for the prepared samples using the spectrum of Degussa P25 TiO<sub>2</sub> as a reference profile. The absorption onset of the doped materials (which are yellow) is pushed further toward the visible region compared with P25 (which is white). Absorption onsets were used to estimate the bandgaps of the various materials, and these are reported in Table 1 using the equation  $E_g = hc/\lambda$ , where  $E_g$  is the band gap energy (J),  $h$  is Planck's constant,  $c$  is the velocity of light, and  $\lambda$  is the wavelength (m) of absorption onset.<sup>23</sup>

It is clear that the presence of the carbon dopant (Figure 4a) increases absorbance toward the visible region. Increasing the nominal concentration of the dopant in the material (by increasing the concentration of melamine borate used during the preparation) had little effect on the position of the absorption onset or the calculated bandgap. (See Table 1.)

Doping with W also increased the absorbance in the visible region (see Figure 4b), but in this case there seems to be an inverse relationship between the extent of W doping and the bandgap; that is, the bandgap decreases as the [W] is increased. This relatively minor effect varies from a decrease of 0.07 eV in undoped catalysts when [W] doping is changed from 1 to 10% to a decrease of up to 0.27 eV for similar W doping levels in samples that nominally had 4% C.

The extents of the increases seen in visible-light absorption are comparable when either W or C is used as dopant



**Figure 4.** Diffuse reflectance UV–visible spectra of (a) TiO<sub>2</sub> (full line) and a C-doped TiO<sub>2</sub> sample nominally containing 4% C (dashed line), (b) TiO<sub>2</sub> (full line) and W-doped TiO<sub>2</sub> containing 1 (●), 5 (■) and 10% (▲) W, and (c) TiO<sub>2</sub> (full line), C-doped TiO<sub>2</sub> (nominally containing 4% C) (●), W-doped TiO<sub>2</sub> containing 1% W (▲), and codoped TiO<sub>2</sub> nominally containing 4% C and 1% W (■).

(compare Figure 4a,b). Co-doping, as expected from recent theoretical calculations,<sup>35</sup> further increases the fraction of visible light that is absorbed. (See Figure 4c.) This is reflected in the decreased calculated bandgaps (Table 1) and may be explained by an increase in the energy of the VB upon doping with carbon and a decrease in the energy of the CB upon doping with tungsten.<sup>35</sup>

XPS analysis was carried out to characterize the effect of doping and the chemical nature of the C, Ti, W, and O atoms present at, or close to, the surface of the doped samples. The presence of new C 1s peaks was expected to confirm directly carbon doping, whereas shifts in the Ti 2p and O 1s binding energies (which are reported to confirm lattice distortion<sup>36</sup>) were expected to confirm doping indirectly.

The C 1s regions of the XPS profiles were studied for both the doped and undoped P25 TiO<sub>2</sub>. Initially three peaks were seen at binding energies of 284.8, 286.2, and 288.7 eV. The peak at 284.8 eV is an instrumental artifact related to elemental adventitious carbon<sup>37</sup> present in all XPS measurements. The peaks at 286.2 and 288.7 eV have previously been related in the literature to interstitial carbonate dopants as well as oxidized carbon species adsorbed on the surface of the material.<sup>18,34,38–40</sup> These peaks were found to be present in both the doped and

undoped samples and must simply be related to carbon contaminants on the surface of the samples. We therefore cannot derive any conclusions on the existence of doping from the binding energies of the electrons related to these C 1s core levels.

XPS analysis of the C-doped and undoped samples was then carried out after sputtering samples for 8 min with low-energy Ar ions (2 keV), followed directly by sputtering for 5 min with high energy Ar ions (4 keV). The purpose of this treatment was to remove adsorbed carbon contaminants by etching away the top surface layers of the material. The peak at 284.8 eV, that is, the instrumental artifact (see above), remained in the spectra of all samples. However, the intensity of the C 1s peaks at 286.2 and 288.7 eV (relating to carbonate species) decreased continually upon sputtering (Figure 5). A new peak at 282.1 eV

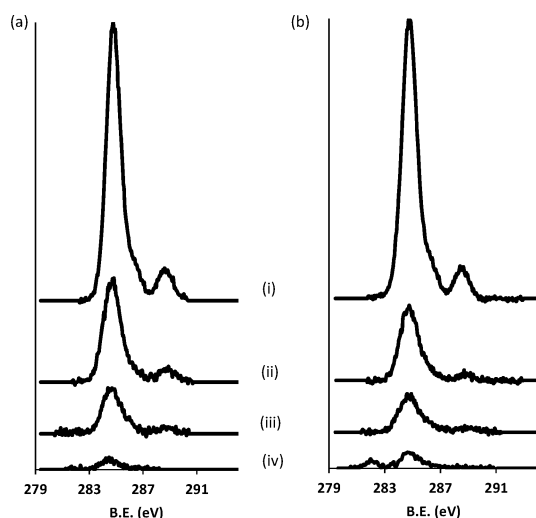


**Figure 5.** XPS C 1s peaks of (a)  $\text{TiO}_2$  and (b) C-doped  $\text{TiO}_2$  (with a nominal loading of 4%) (i) before sputtering, (ii) after sputtering with 2 keV  $\text{Ar}^+$  ions for 2 min, (iii) after sputtering with 2 keV  $\text{Ar}^+$  ions for 8 min, and (iv) after sputtering with 2 keV  $\text{Ar}^+$  ions for 8 min and 4 keV  $\text{Ar}^+$  ions for 5 min. Note the emergence of a new peak at 282 eV in the sample that had been doped with C.

was revealed in the carbon-doped sample after sputtering. This peak is observed only after removal of the masking carbonate species (present in the top layer of the sample) and has been related to Ti–C or carbon substitutionally doped in the place of oxygen in the  $\text{TiO}_2$  lattice<sup>41–44</sup> in literature.

The carbon dopant concentration, as measured using XPS, was determined from the intensity of the carbide C 1s peak at 282.1 eV. The undoped  $\text{TiO}_2$  (after sputtering for 8 min with low-energy Ar ions (2 keV)) contained 0 atom % carbon, whereas the doped  $\text{TiO}_2$  material studied contained 0.5 atom % carbon. Total surface carbon content including adventitious surface-adsorbed elemental carbon and carbonate species (before sputtering) as measured using XPS was naturally higher again (25.6 atom % for the undoped and 27 atom % for the C-doped material). This measured carbon level (0.5 atom % (or 0.225 mass %)) for the sputtered  $\text{TiO}_2$  materials suggests that there is surface enrichment of carbon on these samples as the elemental analysis results showed only 0.03 mass % carbon in the entirety of this particular sample.

Before sputtering, as was expected, two peaks were observed in the Ti 2p region related to ejection of electrons from Ti  $2p_{3/2}$  and Ti  $2p_{1/2}$  levels. The Ti  $2p_{3/2}$  binding energy for the

undoped  $\text{TiO}_2$  sample was 458.3 eV. The Ti  $2p_{3/2}$  binding energy for the C-doped  $\text{TiO}_2$  samples was 458.6 eV, an increase of 0.3 eV. The Ti  $2p_{1/2}$  binding energy for the undoped P25 (Degussa)  $\text{TiO}_2$  sample was 464.0 eV, whereas the analogous peak for the C-doped sample was 464.4 eV, again an increase but this time of 0.4 eV. In both cases, the binding energy increases upon C-doping (Figure 6). This may indicate lattice distortions.

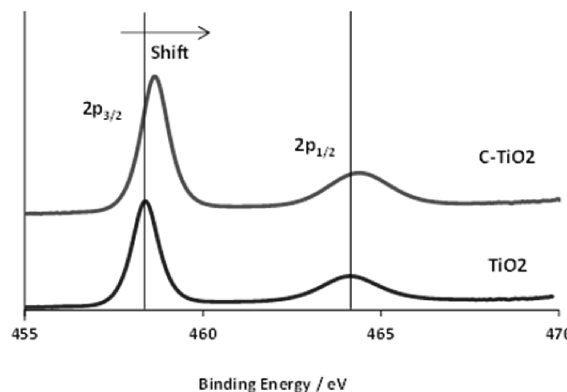


**Figure 6.** XPS Ti 2p peaks of  $\text{TiO}_2$  and C-doped  $\text{TiO}_2$  (with a nominal loading of 4%). Note the increase in the Ti 2p binding energy upon C-doping.

There were also two peaks observed in the O 1s region related to oxide and hydroxyl oxygen. The O 1s binding energies for the C-doped samples, when compared with the O 1s binding energies of undoped P25 (Degussa), also displayed a slight shift. This was from 529.6 eV in the undoped  $\text{TiO}_2$  materials to 529.9 eV in the doped sample and from 530.9 in the undoped to 531.5 in the doped sample. Again, this may indicate lattice distortion upon doping.

The tungsten-containing materials displayed two peaks in the W 4d region related to ejection of electrons from W  $4d_{5/2}$  and W  $4d_{3/2}$  levels at 247.2 and 259.7 eV (Supporting Information, Figure S1) and a peak at 36.6 eV due to electron ejection from the W 4f level. These readings are consistent with literature reports on tungsten-doped  $\text{TiO}_2$ .<sup>27,45</sup>

Furthermore, the N 1s and B 1s regions of the XPS spectra were studied to investigate the possibility of N and B present as additional dopants from the melamine borate. Neither N 1s peaks ( $\sim 400$  eV) nor B 1s peaks ( $\sim 190$  eV) were observed (Supporting Information, Figures S2 and S3, respectively). This shows (perhaps surprisingly) that despite the high N content in melamine (and the  $\text{NH}_4\text{OH}$  used during the preparation) little or no N was incorporated into the  $\text{TiO}_2$  as a dopant. It is evident that during the solution processing and the subsequent washing, filtering, and calcination steps these elements are removed as side-products.

These results contrast somewhat with those in recent literature reports where Kisch et al.<sup>46</sup> investigated the nature of N-doped/modified  $\text{TiO}_2$  formed from urea or melamine. They found that a key step in the formation N-doped/modified  $\text{TiO}_2$  from this precursor was the  $\text{TiO}_2$ -catalyzed formation of melamine, followed by various self-condensations to form a mixture of oligo-nuclear aromatic amines. This was followed by further condensation between the triazine amino groups of these molecules and surface hydroxyl species on  $\text{TiO}_2$  to generate Ti–N bonds. These materials then showed activity in promotion of the photo-decomposition of formic acid under visible-light irradiation. The authors suggest that neither nitridic species, nor  $\text{NO}_x$

species, nor  $\text{TiO}_2$  defect states are responsible for this reactivity but rather melamine condensation products acting as visible-light sensitizers.

The authors clearly show N-doping of their  $\text{TiO}_2$  materials when using melamine as a dopant, in contrast with the results shown here (where only C-doping is observed). However, there are several differences in the synthesis procedures used in the preparation of our materials and those of Kisch et al.<sup>46</sup> First, in ref 46, the levels of melamine used were significantly higher in their case (with catalyst/melamine ratios of 1:2) compared with our case, where we would have a vast excess of  $\text{TiO}_2$  precursor compared with organic material. Second, and more importantly, Kisch's materials were produced by grinding preformed  $\text{TiO}_2$  with urea or melamine/melamine derivatives, followed by calcination. The melamine (or melamine condensation products) are attached to the surface of the  $\text{TiO}_2$  through condensation with surface hydroxyl groups. The materials prepared here are produced by introducing melamine into the pre- $\text{TiO}_2$  sol (via a melamine borate solution) before hydrolysis and condensation of the sol to form  $\text{TiO}_2$ . Any melamine not incorporated into the pre- $\text{TiO}_2$  lattice is removed via washing and filtration before drying and calcination. There is no opportunity for high levels of the surface condensation reactions seen in ref 46.

Photocatalytic experiments were carried out to study whether the increased light absorption also resulted in an increased photocatalytic activity. The photocatalytic degradation of 4-chlorophenol in the presence of the photocatalysts under visible light ( $\lambda > 410$  nm) was investigated by determining the remaining levels of dissolved organic carbon-containing compounds at various time intervals following initiation of the reaction. Chlorophenols are ideal model compounds for characterizing the photocatalytic activity of pristine and doped  $\text{TiO}_2$ . TOC measurements have previously shown that they undergo total mineralization by  $\text{TiO}_2$  photocatalysts.<sup>47,48</sup>

Figure 7 shows the degradation versus time profiles for the photocatalytic oxidation of chlorophenol under visible light

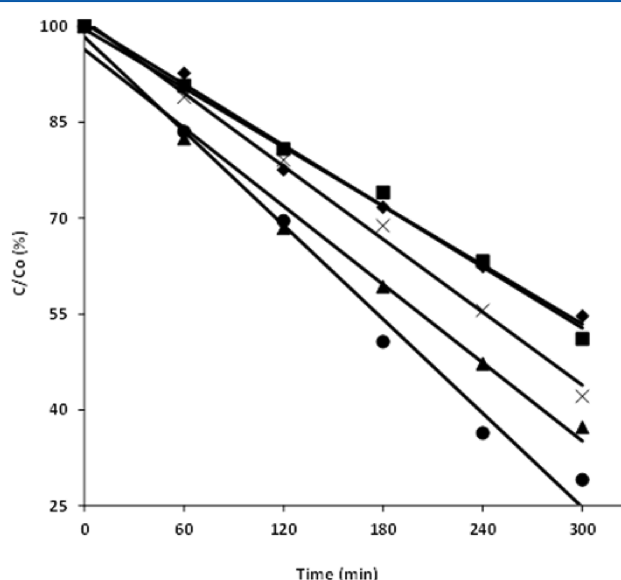


**Figure 7.** Photocatalytic degradation (as determined by TOC analysis) of 4-chlorophenol under visible-light irradiation by P25  $\text{TiO}_2$  (□), C- $\text{TiO}_2$  with nominal 4% C loading 1 h calcination (●), 3 h of calcination (▲), 1% W- $\text{TiO}_2$  (■), and codoped C,W- $\text{TiO}_2$  with 1% W loading and nominal 4% C loading (×).

only (determined using TOC analysis). It is clear that carbon-doped  $\text{TiO}_2$  material calcined for 1 h shows the highest photocatalytic ability, degrading ~71% of the chlorophenol in 300 min. A carbon-doped  $\text{TiO}_2$  sample that had been calcined for 3 h was less effective, degrading ~63% of the initial concentration of chlorophenol in the same time interval, despite this being a more crystalline material<sup>49</sup> and having a smaller band gap. (See Table 1.) The photocatalytic degradation process is reportedly heavily influenced by morphology, phase, chemical composition, and particle size.<sup>50–53</sup> The smaller crystalline particle size and increased surface area of the material calcined for only 1 h appear to have enhanced the photocatalytic activity.

Degussa P25  $\text{TiO}_2$  also performed reasonably well in these measurements, degrading 56% of chlorophenol in 300 min (despite the fact that the experiments took place in the presence of visible light only). The UV filter film used cuts off light <410 nm, and from Figure 4, it is clear that P25  $\text{TiO}_2$  can absorb relatively small amounts of light (generating electron hole pairs) above this wavelength. The observed activity confirms the well-known photocatalytic activity of P25 due to the high crystallinity and the inherent optimal anatase/rutile ratio existing in this grade of  $\text{TiO}_2$ .

Furthermore, even though neither  $\text{TiO}_2$  nor chlorophenol (CP) absorbs visible light, it has been reported that the  $\text{TiO}_2$ –CP<sub>ads</sub> system has charge-transfer bands that can absorb such radiation.<sup>54–57</sup> Kim and Choi have shown that charge carriers can be generated from the excitation of these charge-transfer states and that there remains the possibility for a variety of photochemistries to result from reaction of these charge carriers. Gray et al.<sup>55,56</sup> have demonstrated visible-light activity for the reaction of a range of chlorophenols following excitation of these charge-transfer bands. These authors have also pointed out that full mineralization of the adsorbed species requires UV light (because the CT complex is destroyed by the first electron transfer step) but that the initial degradation (involving  $\text{Cl}^-$  formation) can proceed using visible light. Of course this process would also operate in the doped catalysts. It is then evident that the initial intermediate oxidation product can undergo further solution-based homogeneous reactions involving free radicals.

As predicted by theoretical calculations<sup>35</sup> and as shown by UV–vis spectroscopy here (see Figure 4c), the C,W-codoped material had an absorbance significantly shifted toward the visible region. However, despite the enhanced optical properties of the W-doped and codoped  $\text{TiO}_2$  catalysts, these were considerably poorer photo-oxidation catalysts (see Figure 4c) compared with C- $\text{TiO}_2$  materials. This may be due to W cations acting as electron hole recombination centers due to the introduction of isolated localized d states below the CB.<sup>58–60</sup>

Recently, codoping of  $\text{TiO}_2$  has been reported to passivate localized defect bands that may be present in monodoped  $\text{TiO}_2$  such that they no longer act as recombination centers.<sup>61</sup> Codoping carbon and tungsten has been reported to yield such a passivation effect in comparison with singly doped tungsten or carbon  $\text{TiO}_2$ . This reported passivation is due to the formation of a C 2p–W 5d hybridized band<sup>35</sup> when dopants are located near one other (as the nearest neighbor or the second nearest neighbor). This strengthens hybridization between C 2p and O 2p, resulting in a fully occupied band of higher energy than the top of the VB edge and at the same time forms a continuum-like band between the CB and tungsten dopant d states below. This should result in enhanced photocatalytic activity in codoped (as compared with singly doped) materials due to



improved charge-carrier mobility and reduced electron hole recombination. There may be some evidence of passivation of this effect by the carbon because the codoped C,W-TiO<sub>2</sub> performs better than singly doped W-TiO<sub>2</sub>. However, the activity of the codoped sample is still lower than that of singly doped C-TiO<sub>2</sub>.

This discrepancy between the predicted and observed behavior may simply be due the locations of the dopants situated further from one other in the lattice and the presence of relatively low levels of carbon dopant. (It was also reported that when the carbon and tungsten dopants are far from each other in the lattice the passivation effect should no longer exist.<sup>35</sup>)

Therefore, it seems that there are sufficient levels of carbon and tungsten to increase absorbance toward the visible region but insufficient carbon located near the tungsten dopant to passivate recombination effects due to tungsten incorporation. Overall, this results in a net decreased photocatalytic activity.

This result confirms that the performance of a material as a solar photocatalyst is not a function of solely the ability of the material to absorb light in the visible region of the spectrum. Other factors are also important such as the crystallinity and particle size of the material and the ability of the material to retard the electron–hole recombination process.<sup>50–53,58–60</sup>

Many reported photocatalytic studies have repeatedly shown that the enhanced visible-light absorption observed in the UV–vis spectra of catalysts does not translate into increased visible-light-induced photocatalytic activity. This, in fact, has stagnated this field of research for more than a decade. Most reported studies involving doped TiO<sub>2</sub> photocatalysts propose that the observed red shift in light absorption is caused by a narrowing of the band gap of pristine TiO<sub>2</sub> or due to the appearance of intragap localized states of the dopants without considering the possibility of forming color centers that absorb in the visible-light spectral region, as recently shown by Kuznetsov and Serpone.<sup>25,62</sup> In the present study, the XPS data clearly show that doping definitely occurs in the TiO<sub>2</sub> lattice. This is also well-reflected in the increased chlorophenol photocatalytic oxidation activity of C-TiO<sub>2</sub> noted under visible-light irradiation. Such beneficial effects are totally absent with the W and C,W-codoped TiO<sub>2</sub>, despite the noticeable red shifts observed in their absorption spectra. The beneficial effect of C-doped samples under solely visible irradiation cannot be the result of any inadvertent UV photon entry into the system because such a process would also have improved the activity of the W and W,C-codoped samples. Also, the theoretically predicted advantage for photocatalysis<sup>35</sup> was not evident with these doped samples despite the effect of doping clearly being seen in the XPS spectra. These aspects need to be clarified for photocatalysis to be properly understood.

On the basis of our results, it is logical to conclude that a significant fraction of the spectral red shift commonly observed with doped catalysts might be due to the formation of color centers as a result of defects associated with oxygen vacancies. However, even though bandgap-related narrowing or intragap localization of dopant levels is possible, it seems that these are not the major factors responsible for enhanced visible-light absorption as commonly reported in this field of research. This also throws light onto the insensitivity of the calculated band-gap values reported in Table 1 (based on spectral absorption thresholds) to the degree of dopant concentration for the various catalysts studied here.

Photocatalytic activity experiments were also carried out under the ‘full sun’ conditions (i.e., in the absence of a UV filter, where the reaction vessels were exposed to the full AM1.5G spectrum). Again the photocatalytic degradation of 4-chlorophenol in the presence of the photocatalysts was investigated using TOC measurements.

Figure 8 shows the degradation versus time profiles for the photocatalytic oxidation of chlorophenol (determined using

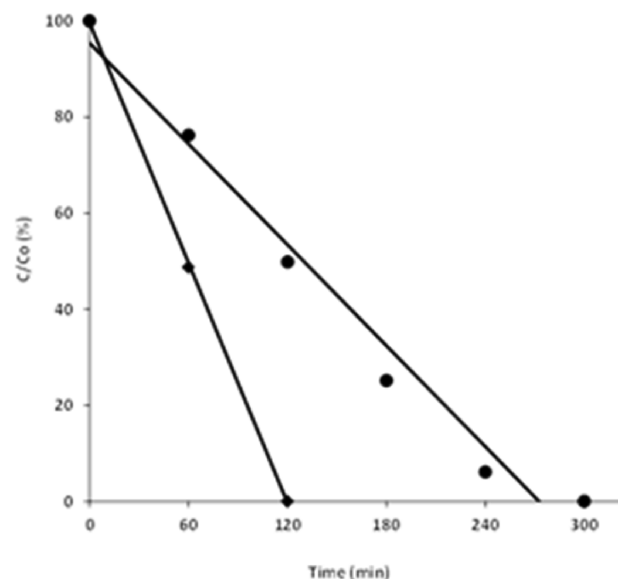
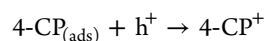


**Figure 8.** Photocatalytic degradation (as determined by TOC analysis) of 4-chlorophenol under UV plus visible-light irradiation by P25 TiO<sub>2</sub> (●) and C-TiO<sub>2</sub> with nominal 4% C loading 1 h calcination (◆).

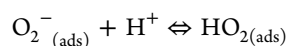
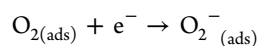
TOC analysis) under UV plus visible light. All materials studied were more active under the ‘full sun’ conditions than they were under the ‘visible-light only’ conditions (see Figure 7), reflecting the increased number of electron hole pairs that can be generated when UV light is available to cause excitation. The order of catalytic activity, however, differs. Under these conditions, P25 TiO<sub>2</sub> degrades all of the chlorophenol within 2 h. C-TiO<sub>2</sub> (calcined for 1 h), while the most active powder in the visible-light experiments (see Figure 7), takes over 4 h to complete the total breakdown of the same levels of chlorophenol.

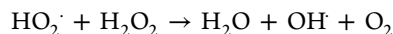
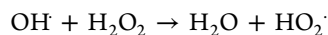
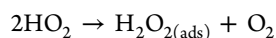
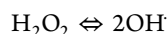
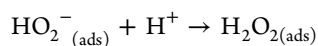
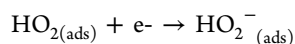
Over TiO<sub>2</sub>, following illumination with the appropriate energies of light and generation and separation of electron hole pairs, degradation of organic species can take place by several different pathways:

- (i) Directly, where the holes accept an electron from an adsorbed species. These holes can exist in the VB of TiO<sub>2</sub> or in higher energy orbitals related to the presence of dopant

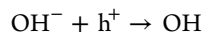


- (ii) Indirectly via OH· radical reactions, where the radicals are formed from O<sub>2</sub><sup>−</sup> species that are generated from the reduction of dissolved O<sub>2</sub> using the promoted electron<sup>63</sup> (as in the reactions shown below).





(iii) Indirectly via the generation of  $\text{OH}^\cdot$  radicals from the oxidation of  $\text{OH}^-$  on VB or dopant level holes.



Under full sun conditions, the undoped  $\text{TiO}_2$  performs better than our carbon-doped  $\text{TiO}_2$  materials despite more photons being available for electron promotion (and reaction initiation) in the latter catalyst. This indicates that the holes formed in the VB of undoped  $\text{TiO}_2$  are more active than those generated in the dopant-related orbitals, and it can be assumed that this in turn relates to the greater driving force (due to the differences in their respective redox levels) involved in neutralizing the VB holes.

Another possible reason for the lower activity of the doped materials may relate to the relative energetics of the holes formed in dopant-related energy levels and the required potential for the formation of OH radicals from hydroxide anions. If these holes arise in the mid gap state in the doped  $\text{TiO}_2$ , then they may exist at oxidation potentials higher than that of the OH radical formation potential ( $\text{OH}^-/\text{OH}^\cdot = 1.9 \text{ V NHE}$ ). If the holes are not energetic enough to extract electrons from  $\text{OH}^-$ , then the generation of these OH radicals will be retarded and one route for 4-CP degradation will be restricted. In an example of this, Park et al.<sup>18</sup> have reported that, following carbon doping the mid-gap level lies somewhere between 1.9 and 1.4 V because they note this effect in the oxidation of 4-CP (1.9 V) with C-doped samples but less of an effect in  $\text{I}^-$  oxidation (where a potential of only 1.4 V is required).

In carbon-doped  $\text{TiO}_2$ , if the mid-gap energy state induced by doping lies at a higher oxidation potential than the OH radical formation potential, then the doped material, despite being able to absorb more photons, will not form OH radicals and promote indirect degradation of the 4-CP. These holes will, however, still degrade 4-CP via direct oxidation because the 4-CP oxidation potential (0.8 V versus NHE) lies above the mid-gap state.

Any advantage derived from being doped (and thus being able to absorb more photons of lesser energy to promote an electron) is negated by the positioning of the mid-gap energy state in relation the OH radical formation potential, and in effect the reaction proceeds mostly via interactions involving  $\text{O}_2^-$ , which is generated in the reductive half reactions.

In our situation, this route is not expected to wield a considerable effect on reactivity because the photocatalytic reactions initially have a pH of 6 (from 4-chlorophenol), and this will fall as mineralization progresses (due to the release of HCl). This would result in low concentrations of free  $\text{OH}^-$  and a low rate of OH radical formation from  $\text{OH}^-$  oxidation.

There is now a general agreement that N-doping need not result in a shift of the VB edge (i.e., a shift in the O 2p states), creating more-or-less localized N 2p states whose energies are

located within the bandgap. Our results with C-doped catalysts also indicate that the doped sites, despite improving the visible-light absorption characteristics, are not directly involved in the photocatalytic decomposition of surface-adsorbed organics, and most of the resulting photocatalysis occurs through  $\text{O}_2^-$ -related solution reactions.<sup>64–69</sup>

Another critical point is that typically C doping leads to extremely low concentrations of C in the structure. We cannot assume that this concentration is sufficient to raise the bulk valence-band level by >0.5 eV, and it is more likely that we are simply adding discrete energy levels at energies somewhat above the upper edge of the VB. If this is the case and holes generated within these energy levels are not suitable for the production of hydroxyl radicals from hydroxide ions, then one major route toward organic degradation is adversely affected.

In any case, it should be noted that in practical applications of photocatalysis, light irradiation is often used to produce only the initial molecular breakdown to biodegradable fragments, and the subsequent total mineralizations are often carried out by relatively less expensive biological processes. This study shows that visible-light-active C-doped photocatalysts prepared through the melamine borate method can perform the initial molecular fragmentation of pollutants (30% TOC removal in 120 min and even up to 71% TOC removal in 300 min) using relatively cheaper and more energy-efficient visible lamps, such as LEDs (with lifetimes of 10 000 h), which require very low running costs. Furthermore, their use in gas-phase depollution of odor-causing vapors in indoor conditions is a clear possibility.<sup>70</sup>

#### 4. CONCLUSIONS

Carbon-doped  $\text{TiO}_2$  photocatalysts were reproducibly formed using an inexpensive and facile altered sol–gel preparation method with melamine borate as an external source of carbon dopant. The materials (which did not contain either N or B dopants) have been shown by XPS to contain carbon substitutionally doped into the  $\text{TiO}_2$  lattice. The carbon-doped  $\text{TiO}_2$  has shown improved optical absorbance and photocatalytic activity under visible light compared with undoped  $\text{TiO}_2$  and Degussa P25. Carbon and tungsten codoped materials have also been formed using this novel carbon doping approach combined with a well-known tungsten doping method.<sup>16</sup>

The addition of tungsten improved the optical absorbance properties of the materials in accordance with reported theoretical calculations, but did not enhance their photocatalytic activity as expected from the theoretical models. This is thought to be mainly due to the effects of recombination of electron–hole pairs at the tungsten metal ion centers. A significant fraction of the enhanced red-shifted light absorption is also thought to arise from color centers associated with oxygen defects in the doped  $\text{TiO}_2$  lattice. For further progress in visible-light-induced photocatalysis to be made, it will be necessary to understand the individual contributions toward spectral red shifts arising from bandgap alterations and the formation of oxygen defect based color centers, respectively.

The activity under whole sun conditions of the materials (while being higher than the activity under visible-light only conditions) is lower than that of P25, suggesting a greater driving force for neutralization of VB holes than for neutralization of dopant level holes. Furthermore, the holes formed following absorbance of lower energy photons are in localized energy levels within the bandgap, and these energies are not sufficient to generate active hydroxyl species. It would not be expected that this constitutes a significant route of reaction.

## ■ ASSOCIATED CONTENT

### ■ Supporting Information

Profiles showing the W4d, W4f, N1s, and B1s regions of the XPS spectra of TiO<sub>2</sub>, C-TiO<sub>2</sub>, and C,W-TiO<sub>2</sub>. This material is available free of charge via the Internet at <http://pubs.acs.org>.

## ■ AUTHOR INFORMATION

### Corresponding Author

\*E-mail: James.Sullivan@ucd.ie (J.A.S.); Ravindranathan.Thampi@ucd.ie (K.R.T.).

### Present Address

<sup>†</sup>UCD School of Chemical and Bioprocess Engineering, Belfield, Dublin 4, Ireland.

### Notes

The authors declare no competing financial interest.

## ■ ACKNOWLEDGMENTS

We acknowledge and thank Science Foundation Ireland for their funding of this Strategic Research Cluster Programme (07/SRC/B1160) and our Industry Partners for their support of this Cluster. We specifically thank SSE Renewables for their support of E.M.N.

## ■ ABBREVIATIONS

C-TiO<sub>2</sub>, carbon-doped TiO<sub>2</sub>; W-TiO<sub>2</sub>, tungsten-doped TiO<sub>2</sub>; C,W-TiO<sub>2</sub>, carbon and tungsten codoped TiO<sub>2</sub>; VB, valence band; CB, conduction band; CP, chlorophenol; CT, charge transfer; TGA, thermogravimetric analysis; MS, mass spectrometry; XRD, X-ray diffraction; XPS, X-ray photoelectron spectroscopy; DRS, diffuse reflectance spectroscopy; TOC, total organic carbon

## ■ REFERENCES

- Hoffmann, M. R.; Martin, S. T.; Choi, W. Y.; Bahnemann, D. W. *Chem. Rev.* **1995**, *95*, 69–96.
- Mills, A.; LeHunte, S. J. *Photochem. Photobiol. A* **1997**, *108*, 1–35.
- Ashokkumar, M. *Int. J. Hydrogen Energy* **1998**, *23*, 427–438.
- Ni, M.; Leung, M. K. H.; Leung, D. Y. C.; Sumathy, K. *Renewable Sustainable Energy Rev.* **2007**, *11*, 401–425.
- Herrmann, J. M. *Catal. Today* **1999**, *53*, 115–129.
- Patsoura, A.; Kondarides, D. I.; Verykios, X. E. *Catal. Today* **2007**, *124*, 94–102.
- Bowker, M.; James, D.; Stone, P.; Bennett, R.; Perkins, N.; Millard, L.; Greaves, J.; Dickinson, A. J. *Catal.* **2003**, *217*, 427–433.
- Kondarides, D. I.; Daskalaki, V. M.; Patsoura, A.; Verykios, X. E. *Catal. Lett.* **2008**, *122*, 26–32.
- Bard, A. J. *J. Photochem. Photobiol. A* **1979**, *10*, 59–75.
- Grimes, C. A.; Varghese, O. K.; Ranjan, S. *Light, Water, Hydrogen: The Solar Generation of Hydrogen by Water Photoelectrolysis*; Springer: New York, 2008.
- Asahi, R.; Morikawa, T.; Ohwaki, T.; Aoki, K.; Taga, Y. *Science* **2001**, *293*, 269–271.
- Chen, D. M.; Jiang, Z. Y.; Geng, J. Q.; Wang, Q.; Yang, D. *Ind. Eng. Chem. Res.* **2007**, *46*, 2741–2746.
- Choi, W. Y.; Termin, A.; Hoffmann, M. R. *Angew. Chem., Int. Ed.* **1994**, *33*, 1091–1092.
- Irie, H.; Watanabe, Y.; Hashimoto, K. *J. Phys. Chem. B* **2003**, *107*, 5483–5486.
- Khan, S. U. M.; Al-Shahry, M.; Ingler, W. B. *Science* **2002**, *297*, 2243–2245.
- Lorret, O.; Francova, D.; Waldner, G.; Stelzer, N. *Appl. Catal., B* **2009**, *91*, 39–46.
- Nakamura, R.; Tanaka, T.; Nakato, Y. *J. Phys. Chem. B* **2004**, *108*, 10617–10620.
- Park, Y.; Kim, W.; Park, H.; Tachikawa, T.; Majima, T.; Choi, W. *Appl. Catal., B* **2009**, *91*, 355–361.
- Sakthivel, S.; Janczarek, M.; Kisch, H. *J. Phys. Chem. B* **2004**, *108*, 19384–19387.
- Shen, X. Z.; Guo, J.; Liu, Z. C.; Xie, S. M. *Appl. Surf. Sci.* **2008**, *254*, 4726–4731.
- Tachikawa, T.; Tojo, S.; Kawai, K.; Endo, M.; Fujitsuka, M.; Ohno, T.; Nishijima, K.; Miyamoto, Z.; Majima, T. *J. Phys. Chem. B* **2004**, *108*, 19299–19306.
- Wang, C. Y.; Bahnemann, D. W.; Dohrmann, J. K. *Chem. Commun.* **2000**, *16*, 1539–1540.
- Yang, X. X.; Cao, C. D.; Erickson, L.; Hohn, K.; Maghirang, R.; Klabunde, K. J. *Catal.* **2008**, *260*, 128–133.
- Zaleska, A. *Recent Pat. Eng.* **2008**, *2*, 157–164.
- Serpone, N. J. *J. Phys. Chem. B* **2006**, *110*, 24287–24293.
- Sakatani, Y.; Ando, H.; Okusako, K.; Koike, H.; Nunoshige, J.; Takata, T.; Kondo, J. N.; Hara, M.; Domen, K. *J. Mater. Res.* **2004**, *19*, 2100–2108.
- Shen, Y. F.; Xiong, T. Y.; Li, T. F.; Yang, K. *Appl. Catal., B* **2008**, *83*, 177–185.
- Wang, D.; Zou, Y. H.; Wen, S. C.; Fan, D. Y. *Appl. Phys. Lett.* **2009**, *95*, 012106.
- Andersson, S.; Collen, B.; Kuylenssterna, U.; Magnéli, A. *Acta Chem. Scand.* **1957**, *11*, 1641–1652.
- Reyes-Coronado, D.; Rodriguez-Gattorno, G.; Espinosa-Pesqueira, M. E.; Cab, C.; de Coss, R.; Oskam, G. *Nanotechnology* **2008**, *19*, 145605.
- Jobbagy, M.; Couselo, N.; Einschlag, F. S. G.; Candal, R. J. *J. Phys. Chem. C* **2008**, *112*, 1094–1100.
- Yang, Y.; Wang, H.; Li, X.; Wang, C. *Mater. Lett.* **2009**, *63*, 331–333.
- Patterson, A. L. *Phys. Rev.* **1939**, *56*, 978–982.
- Sakthivel, S.; Kisch, H. *Angew. Chem., Int. Ed.* **2003**, *42*, 4908–4911.
- Long, R.; English, N. J. *Chem. Mater.* **2010**, *22*, 1616–1623.
- Sun, H. Q.; Bai, Y.; Cheng, Y. P.; Jin, W. Q.; Xu, N. P. *Ind. Eng. Chem. Res.* **2006**, *45*, 4971–4976.
- Papirer, E.; Lacroix, R.; Donnet, J. B.; Nanse, G.; Fioux, P. *Carbon* **1995**, *33*, 63–72.
- Li, Y. Z.; Hwang, D. S.; Lee, N. H.; Kim, S. J. *Chem. Phys. Lett.* **2005**, *404*, 25–29.
- Ohno, T.; Tsubota, T.; Nishijima, K.; Miyamoto, Z. *Chem. Lett.* **2004**, *33*, 750–751.
- Ren, W. J.; Ai, Z. H.; Jia, F. L.; Zhang, L. Z.; Fan, X. X.; Zou, Z. G. *Appl. Catal., B* **2007**, *69*, 138–144.
- In, S. I.; Kean, A. H.; Orlov, A.; Tikhov, M. S.; Lambert, R. M. *Energy Environ. Science* **2009**, *2*, 1277–1279.
- Irie, H.; Washizuka, S.; Hashimoto, K. *Thin Solid Films* **2006**, *510*, 21–25.
- Irie, H.; Watanabe, Y.; Hashimoto, K. *Chem. Lett.* **2003**, *32*, 772–773.
- Hsu, S. W.; Yang, T. S.; Chen, T. K.; Wong, M. S. *Thin Solid Films* **2007**, *515*, 3521–3526.
- Li, X. Z.; Li, F. B.; Yang, C. L.; Ge, W. K. *J. Photochem. Photobiol., A* **2001**, *141*, 209–217.
- Mitoraj, D.; Kisch, H. *Angew. Chem., Int. Ed.* **2008**, *47*, 9975–9978.
- Dhananjeyan, M. R.; Kiwi, J.; Thampi, K. R. *Chem. Commun.* **2000**, 1443–1444.
- Dhananjeyan, M. R.; Mielczarski, E.; Thampi, K. R.; Buffat, P.; Bensimon, M.; Kulik, A.; Mielczarski, J.; Kiwi, J. *J. Phys. Chem. B* **2001**, *105*, 12046–12055.
- Ohtani, B.; Ogawa, Y.; Nishimoto, S. *J. Phys. Chem. B* **1997**, *101*, 3746–3752.
- Binitha, N. N.; Yaakob, Z.; Resmi, R. *Cent. Eur. J. Chem.* **2010**, *8*, 182–187.
- Anpo, M.; Aikawa, N.; Kodama, S.; Kubokawa, Y. *J. Phys. Chem.* **1987**, *91*, 4305–4310.

- (52) Ho, W. K.; Yu, J. C.; Lee, S. C. *J. Solid State Chem.* **2006**, *179*, 1171–1176.
- (53) Bickley, R. I.; Gonzalezcarreno, T.; Lees, J. S.; Palmisano, L.; Tilley, R. J. D. *J. Solid State Chem.* **1991**, *92*, 178–190.
- (54) Kim, S.; Choi, W. *J. Phys. Chem. B* **2005**, *109*, 5143–5149.
- (55) Hurum, D. C.; Gray, K. A.; Rajh, T.; Thurnauer, M. C. *J. Phys. Chem. B* **2004**, *108*, 16483–16487.
- (56) Agrios, A. G.; Gray, K. A.; Weitz, E. *Langmuir* **2003**, *19*, 1402–1409.
- (57) Usseglio, S.; Calza, P.; Damin, A.; Minero, C.; Bordiga, S.; Lamberti, C.; Pelizzetti, E.; Zecchina, A. *Chem. Mater.* **2006**, *18*, 3412–3424.
- (58) Herrmann, J. M.; Disdier, J.; Pichat, P. *Chem. Phys. Lett.* **1984**, *108*, 618–622.
- (59) Lou, Z.; Gao, Q. *Photochem. Photobiol., A* **1992**, *63*, 367–375.
- (60) Umebayashi, T.; Yamaki, T.; Itoh, H.; Asai, K. *J. Phys. Chem. Solids* **2002**, *63*, 1909–1920.
- (61) Gai, Y. Q.; Li, J. B.; Li, S. S.; Xia, J. B.; Wei, S. H. *Phys. Rev. Lett.* **2009**, *102*, 036402.
- (62) Kuznetsov, V. N.; Serpone, N. J. *J. Phys. Chem. B* **2006**, *110*, 25203–25209.
- (63) Vinodgopal, K.; Stafford, U.; Gray, K. A.; Kamat, P. V. *J. Phys. Chem.* **1994**, *98*, 6797–6803.
- (64) Nah, Y.-C.; Paramasivam, I.; Schmuki, P. *ChemPhysChem* **2010**, *11*, 2698–2713.
- (65) Henderson, M. A. *Surf. Sci. Rep.* **2011**, *66*, 185–297.
- (66) Di Valentin, C.; Pacchioni, G.; Selloni, A.; Livraghi, S.; Giamello, E. *J. Phys. Chem. B* **2005**, *109*, 11414–11419.
- (67) Di Valentin, C.; Finazzi, E.; Pacchioni, G.; Selloni, A.; Livraghi, S.; Paganini, M. C.; Giamello, E. *Chem. Phys.* **2007**, *339*, 44–56.
- (68) Finazzi, E.; Di Valentin, C.; Selloni, A.; Pacchioni, G. *J. Phys. Chem. C* **2007**, *111*, 9275–9282.
- (69) Graciani, J.; Alvarez, L. J.; Rodriguez, J. A.; Sanz, J. F. *J. Phys. Chem. C* **2008**, *112*, 2624–3261.
- (70) Kandavelu, V.; Kastien, H.; Thampi, K. R. *Appl. Catal., B* **2004**, *48*, 101–111.